ADVANCED MATERIALS INTERFACES
www.advmatinterfaces.de

Check for updates

# Electronic Characteristics of Ultra-Thin Passivation Layers for Silicon Photovoltaics

*Sophie L. Pain,* Edris Khorani, Tim Niewelt, Ailish Wratten, Galo J. Paez Fajardo, Ben P. Winfield, Ruy S. Bonilla, Marc Walker, Louis F. J. Piper, Nicholas E. Grant, and John D. Murphy**

**Surface passivating thin films are crucial for limiting the electrical losses during charge carrier collection in silicon photovoltaic devices. Certain dielectric coatings of more than 10 nm provide excellent surface passivation, and ultra-thin (<2 nm) dielectric layers can serve as interlayers in passivating contacts. Here, ultra-thin passivating films of $SiO_2$, $Al_2O_3$, and $HfO_2$ are created via plasma-enhanced atomic layer deposition and annealing. It is found that thin negatively charged $HfO_2$ layers exhibit excellent passivation properties—exceeding those of $SiO_2$ and $Al_2O_3$—with 0.9 nm $HfO_2$ annealed at 450 °C providing a surface recombination velocity of 18.6 cm $s^{-1}$. The passivation quality is dependent on annealing temperature and layer thickness, and optimum passivation is achieved with $HfO_2$ layers annealed at 450 °C measured to be 2.2–3.3 nm thick which give surface recombination velocities ≤2.5 cm $s^{-1}$ and $J_0$ values of ≈14 fA $cm^{-2}$. The superior passivation quality of $HfO_2$ nanolayers makes them a promising candidate for future passivating contacts in high-efficiency silicon solar cells.**

## 1. Introduction

Crystalline silicon (c-Si) is the backbone of today's photovoltaics industry, accounting for over 95% of current commercial production.[1] Passivated emitter and rear cell (PERC) silicon solar cells are the industry standard, despite having the disadvantage of metal electrodes directly contacting the silicon, thereby leading to trap-assisted recombination and hence, a reduction in collection of photogenerated charge carriers.[2,3] To improve on PERC technologies and get even closer to the theoretical single-junction efficiency limit, electrical losses in the contacted regions must be reduced.[3–5] Passivating contacts can help alleviate such losses by simultaneously suppressing the current of non-collected carriers to the contact, and by reducing recombination sites at the interface. Introducing a passivating interlayer between the metal/silicon interface provides a route to reducing the recombination current density, $J_0$,[6,7] thereby increasing device voltage.[3]

Passivating contacts have achieved some success to date, with the strongest candidates being polysilicon on top of thin silicon oxide layers (e.g., tunnel oxide passivating contacts (TOPCon) or poly silicon on oxide (POLO)) and amorphous silicon (a-Si) heterojunctions.[3,7,8] TOPCon is an efficient electron-selective contact but has a high thermal budget with temperatures around 900 °C needed to reduce the contact resistivity to acceptable levels.[9] An efficient hole-selective layer that can match or exceed the performance of the current electron-selective materials would be of considerable interest. The use of $SiO_2$-based hole-selective contacts has so far failed to reach equivalent levels.[10,11] The most promising hole-selective contacting materials are *p*-type a-Si and silicon-rich SiC, but conventional high-temperature Ag screen printing methods are not necessarily compatible with such contacts.[10]

S. L. Pain, E. Khorani, T. Niewelt, A. Wratten, B. P. Winfield, N. E. Grant, J. D. Murphy
School of Engineering
University of Warwick
Coventry CV4 7AL, UK
E-mail: sophie.pain@warwick.ac.uk; john.d.murphy@warwick.ac.uk
T. Niewelt
Fraunhofer Institute for Solar Energy Systems ISE
Heidenhofstraße 2, 79110 Freiburg, Germany

The ORCID identification number(s) for the author(s) of this article can be found under https://doi.org/10.1002/admi.202201339.

© 2022 The Authors. Advanced Materials Interfaces published by Wiley-VCH GmbH. This is an open access article under the terms of the Creative Commons Attribution License, which permits use, distribution and reproduction in any medium, provided the original work is properly cited.

DOI: 10.1002/admi.202201339

T. Niewelt
Institute for Sustainable Systems Engineering
University of Freiburg
Emmy-Noether-Straße 2, 79110 Freiburg, Germany
G. J. Paez Fajardo, L. F. J. Piper
Warwick Manufacturing Group
University of Warwick
Coventry CV4 7AL, UK
R. S. Bonilla
Department of Materials
University of Oxford
Parks Road, Oxford OX1 3PH, UK
M. Walker
Department of Physics
University of Warwick
Coventry CV4 7AL, UK

21967350, 2022, 28, Downloaded from https://onlinelibrary.wiley.com/doi/10.1002/admi.202201339 by Oxford University, Wiley Online Library on [21/09/2023]. See the Terms and Conditions (https://onlinelibrary.wiley.com/terms-and-conditions) on Wiley Online Library for rules of use; OA articles are governed by the applicable Creative Commons License

To facilitate significant charge carrier transport, films used for passivating contacts have to be substantially thinner (≪5 nm)[4,12] than those used for conventional passivation which is often tens of nanometers thick.[13–19] Depending on the film thickness, charge carrier transport is understood to be due to either quantum tunneling or via pinholes.[10,20,21] In addition to being thin, passivating contacts must also provide charge-carrier selectivity[4,22,23] and have suitable optical properties.[24] The fixed charges responsible for field-effect passivation in dielectrics also yield carrier selectivity, with negatively charged films such as $Al_2O_3$ being favorable for hole-selective contacts,[4] and positively charged $SiO_2$ being more suitable for electron-selective contacts.[25] This type of selectivity arises from the charge-induced electrostatic potential modifying the charge carrier profile at the dielectric/silicon interface.

Dielectric coatings which have been shown to passivate c-Si effectively could provide a good starting point for the development of passivating contacts. In most cases, surface passivation is realized by a combination of chemical passivation of dangling bonds and field-effect passivation to repel carriers away from the interface. $SiO_2$—the most researched passivation layer for silicon[26]—is commonly grown thermally or via plasma-enhanced chemical vapor deposition. $SiO_2$ possesses positive fixed charges with a density of the order of $\approx 10^{11}$ q cm$^{-2}$.[15,16,27–29] $Al_2O_3$ is known to possess negative fixed charges ($\approx 10^{12}$–$10^{13}$ q cm$^{-2}$),[18,28] in contrast to many common dielectric passivating layers, which are positively charged.[30] Several recent studies have identified $HfO_2$ as a potential passivating layer,[14,31,32] due to its high dielectric constant, thermal stability, and electrical properties.[19] $HfO_2$ passivation studies have achieved a surface recombination velocity (SRV) <10 cm s$^{-1}$ (compared to <2 cm s$^{-1}$ for $SiO_2$[26] and <1 cm s$^{-1}$ for $Al_2O_3$[18,28]) with film thicknesses of 10–20 nm,[13,14,19,31–34] with the lowest SRV (1.2 cm s$^{-1}$) reported by Gougam et al.[33] There are conflicting reports on the polarity of the fixed charge in $HfO_2$ films,[13,14,19,31–34] with charge magnitude commonly reported to be in the $10^{11}$–$10^{12}$ q cm$^{-2}$ range.[14,19,34]

This paper demonstrates that ultra-thin (<3 nm) oxides ($SiO_2$, $Al_2O_3$, and $HfO_2$) grown by atomic-layer deposition (ALD) can act as highly effective passivation layers. We conduct a detailed investigation to determine the optimal processing conditions to maximize the passivation level, the charge polarity, and magnitude in each case. We find that thin $HfO_2$ layers provide excellent passivation while being processed at relatively low temperatures. Such ultra-thin $HfO_2$ layers outperform ultra-thin $Al_2O_3$ films while also having negative charge polarity, suggesting they have potential for further investigation as potential hole-selective contacts in future passivating contact solar cell structures.

## 2. Results

Ultra-thin films of $SiO_2$, $Al_2O_3$, and $HfO_2$ were deposited at 200 °C via ALD with $O_2$ plasma from bis(diethylamido)silane, trimethylaluminum, and tetrakis(dimethylamido)hafnium precursors, respectively. In order to achieve films of 1–2 nm thickness, 20, 5, and 10 ALD cycles were performed for $SiO_2$, $Al_2O_3$, and $HfO_2$, respectively, based on reported growth rates ($SiO_2$: ≈0.6 Å per cycle, $Al_2O_3$: ≈1.3 Å per cycle, $HfO_2$: ≈1.1 Å per cycle).[35] We determined the thickness and stoichiometry of the films at the nm-scale using X-ray photoelectron spectroscopy (XPS), as other techniques such as ellipsometry are challenging to use accurately for such thin layers. Thickness determination was generally conducted on XPS spectra of annealed samples, except in the case of $HfO_2$. $HfO_2$ thicknesses were determined from spectra of as-deposited samples, as the photoelectron sampling depth for annealed $HfO_2$ was found to be considerably lower than the as-deposited case. This is discussed further in Section S1, Supporting Information. Representative XPS spectra of each film are shown in **Figure 1**, with survey scans shown in Figure 1a. Core level peaks in the survey scans are identified in Figure S2, Supporting Information.

The relative intensities of the overlayer peaks (Si *2p* oxide in Figure 1b, Al *2p* in Figure 1c, and Hf *4f* in Figure 1e) and the substrate peaks (elemental Si *2p* in Figure 1b,d,f) were used to determine film thickness. Si *2p* signal corresponding to an oxide is observed for all three materials (as shown in Figure 1b,d,f), indicating the presence of an interfacial $SiO_2$ layer, which would be expected for dielectrics grown under these conditions.[13,18,36]

Thicknesses were determined via the thickogram method,[37] with parameters used in the calculation and the calculated thicknesses summarized in **Table 1**. Calculated thicknesses are 2.2, 0.7, and 0.9 nm for $SiO_2$, $Al_2O_3$, and $HfO_2$. Thicknesses calculated using this method have an estimated uncertainty of ±10%, based on the uncertainty in the attenuation length.[37] The thickness observed for $SiO_2$ and $Al_2O_3$ is greater than would be expected from the expected growth rate, but $SiO_2$ and $Al_2O_3$ layers of this thickness have previously been incorporated into passivating contacts,[38,39] with ultra-thin films contributing to good passivation.[39,40]

These thicknesses are within the range required for passivating contacts[4] and we next assess the passivating ability of each coating. To activate the passivation, samples coated with $SiO_2$, $Al_2O_3$, and $HfO_2$ on both sides were annealed in a tube furnace at set temperatures between 350–700 °C in air. The resulting layers passivated silicon to varying extents, as demonstrated by post-anneal effective lifetime ($\tau_{eff}$) measured via photoconductance decay shown in **Figure 2**. The figure also compares the ultra-thin layers to those of a more conventional thickness of 20 nm.

The injection dependence of the lifetime for thin $SiO_2$ (Figure 2a) is different from that of $Al_2O_3$ (Figure 2b) and $HfO_2$ (Figure 2c). For all annealing temperatures, thin $SiO_2$ films provided only modest passivation, and are substantially worse than the other two. This is in keeping with other reports of ALD-grown $SiO_2$ films, such as the work of Dingemans et al., which reports ALD $SiO_2$ films give rise to significantly higher SRVs than equivalent $Al_2O_3$ films.[43] SRVs for all thin films can be found in Table S4, Supporting Information. The trend in passivation quality with annealing temperature for ultra-thin coatings is mirrored for thicker films, as demonstrated in Figure 2e.

The passivation level of thin $Al_2O_3$ exhibits a clear dependence on annealing temperature. There is also evidence for a change in the mechanism of passivation following annealing at temperatures >500 °C, based on the differing shape of the lifetime curves. It is well established that thicker ALD $Al_2O_3$ films have


© 2022 The Authors. Advanced Materials Interfaces published by Wiley-VCH GmbH

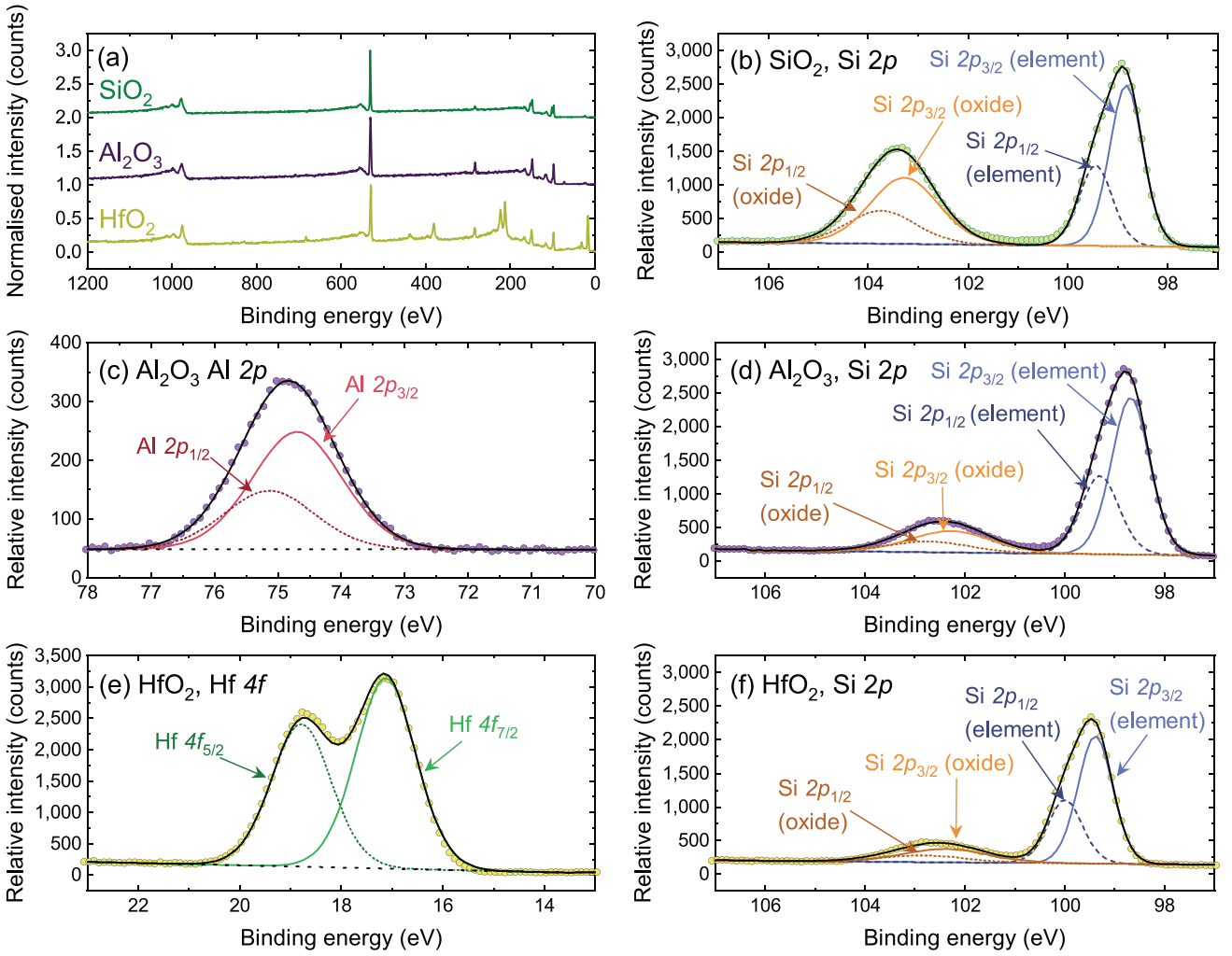


**Figure 1.** XPS spectra for 5 Ω cm *n*-type silicon wafers coated with $SiO_2$, $Al_2O_3$, and $HfO_2$. a) Survey scans; b) Si *2p* peak from $SiO_2$; c) Al *2p* and d) Si *2p* peaks from $Al_2O_3$; and e) Hf *4f* and f) Si *2p* peaks from $HfO_2$.

to undergo an "activation anneal" at ≈450 °C for good passivation to be achieved.[15,16,45] This is confirmed in Figure 2e, which summarizes $\tau_{eff}$ extracted at a carrier density of $1 \times 10^{15}$ $cm^{-3}$ for ≈20 nm of $Al_2O_3$, annealed in the same temperature range. The passivation quality achieved for 20 nm $Al_2O_3$ films is several orders of magnitude greater than for ultra-thin films, with the effective lifetime achieved on annealing at 450 °C approaching the intrinsic lifetime limit, as demonstrated in Figure S3, Supporting Information.[46] This increasing passivation quality with thickness is in keeping with reports on the thickness dependence of $Al_2O_3$.[18] However, at ≈0.7 nm thickness, this activation only occurred on annealing at temperatures >500 °C. Hiller et al. report high-quality surface passivation is achievable for $Al_2O_3$ layers of this thickness, but this improved passivation was achieved via a rapid thermal anneal at 825 °C, and a subsequent forming gas anneal,[39] rather than the lower temperatures and air anneal used in this work.

The passivation level achieved with thin $HfO_2$ is also strongly dependent on annealing temperature, as shown in Figure 2e. Although for $Al_2O_3$ there was a change in the injection dependence of the lifetime curves with annealing temperature, there is no such change for $HfO_2$. Hence it does not seem that there is

**Table 1.** Parameters used in the thickogram calculation for film thickness. $I_0$ and $I_s$ are the relative intensities of the overlayer and substrate peaks, respectively. $S_0$ and $S_s$ are sensitivity factors, and $E_0$ and $E_s$ are the kinetic energy of the overlayer and substrate peaks, respectively.

| Parameter | $SiO_2$ (20 cycles) | $Al_2O_3$ (5 cycles) | $HfO_2$ (10 cycles) |
|---|---|---|---|
| $I_o$ (overlayer) | 2593.3 | 546.4 | 7993.1 |
| $I_s$ (substrate) | 3067.1 | 3397.6 | 2506.8 |
| $S_0$ | 0.772 | 0.505 | 7.12 |
| $S_S$ | 0.772 | 0.772 | 0.772 |
| $E_0$ [eV] | 1383.4 | 1411.9 | 1469.5 |
| $E_S$ [eV] | 1387.9 | 1388.0 | 1387.2 |
| Attenuation length of photoelectrons in overlayer [nm][41,42] | 3.7 | 3.27 | 2.17 |
| **Calculated thickness [nm]** | **2.2** | **0.7** | **0.9** |


© 2022 The Authors. Advanced Materials Interfaces published by Wiley-VCH GmbH

21967350, 2022, 28, Downloaded from https://onlinelibrary.wiley.com/doi/10.1002/admi.202201339 by Oxford University, Wiley Online Library on [21/09/2023]. See the Terms and Conditions (https://onlinelibrary.wiley.com/terms-and-conditions) on Wiley Online Library for rules of use; OA articles are governed by the applicable Creative Commons License

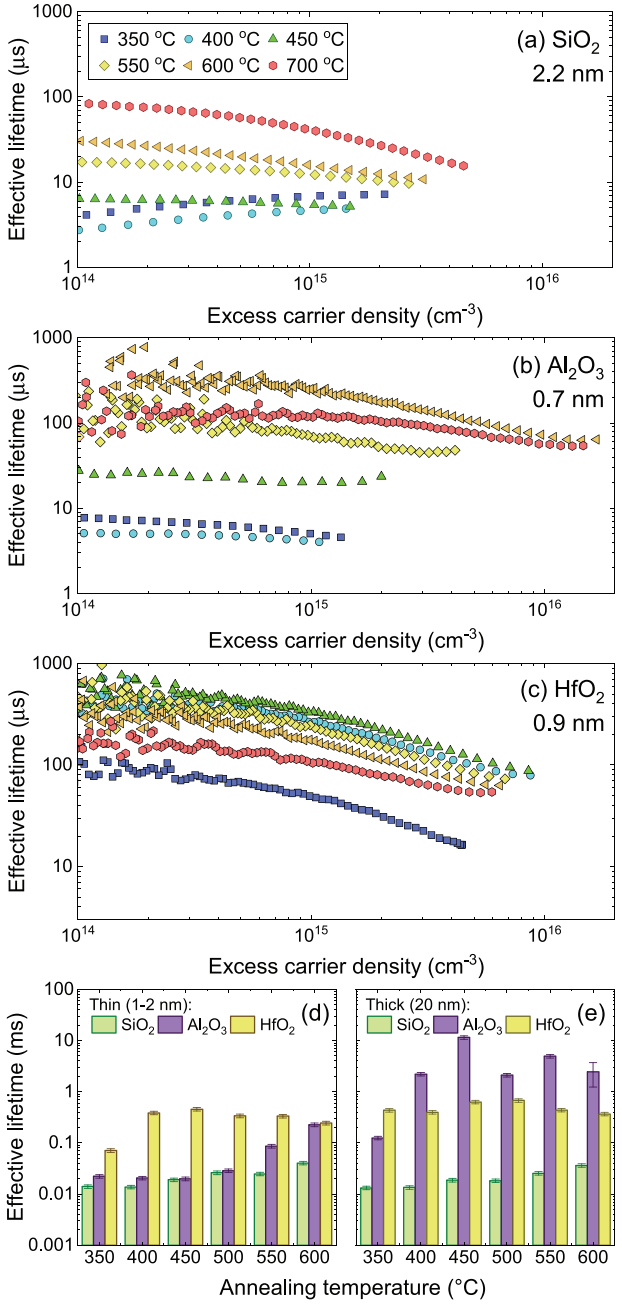


**Figure 2.** Effective lifetime versus excess carrier density for ≈125 µm thick 5 Ω cm *n*-type silicon wafers passivated with a) 2.2 nm $SiO_2$, b) 0.7 nm $Al_2O_3$, and c) 0.9 nm $HfO_2$. Effective lifetime curves are the average of five measurements. Comparison of effective lifetimes at an excess carrier density of $1 \times 10^{15}$ $cm^{-3}$ for $SiO_2$, $Al_2O_3$, and $HfO_2$ at film thicknesses of d) 0.7–2.2 nm, and e) ≈20 nm. Effective lifetime values are assumed to be accurate to ±8%.[44] Error bars for thick $Al_2O_3$ annealed at 600 °C are larger to account for sample inhomogeneity.

a change in the mechanisms responsible for $HfO_2$ passivation (i.e., chemical or field-effect) with annealing temperature. Effective lifetimes initially increase with annealing temperature, peaking at 450 °C before degrading. The increase in lifetimes between 350–450 °C coincides with previously reported crystallization of the $HfO_2$ film, although this was observed for thicker films and the relationship between crystallinity and passivation quality is debated.[13,31,32] The highest quality passivation was achieved at 450 °C, in keeping with other studies which report optimum passivation at temperatures between 350–475 °C.[13,14,31] Above 450 °C, there is clear degradation of the $HfO_2$ passivation quality. The trend in passivation quality with annealing temperature for ultra-thin samples is mirrored for thicker $HfO_2$ films, as demonstrated in Figure 2e, with similar effective lifetimes achieved for samples of either thickness. Previous work suggests that passivation quality should decrease with film thicknesses greater than ≈15 nm,[13,32] but here the two thicknesses achieve similar passivation.

**Figure 3**a compares $\tau_{eff}$ extracted at an excess carrier density of $1 \times 10^{15}$ $cm^{-3}$ as a function of post-deposition annealing temperature. Of all the thin films, the best performance was achieved with $HfO_2$ annealed at 450 °C. Current passivating contacts often have to be fired at temperatures ≥900 °C to achieve reasonable passivation quality.[9] This work shows that it is possible to achieve good quality passivation with $HfO_2$ without needing to anneal at such high temperatures and without the presence of an a-Si heterojunction, hence providing a potential route to lower thermal budget processing while maintaining contact stability.

One way by which passivating contacts can achieve carrier selectivity is via the presence of fixed charge.[4] Consequently, it is necessary to understand the effects of any charge present in the ultra-thin films. The charge polarity can be assessed from the direction of shift under illumination when making surface photovoltage (SPV) measurements using a Kelvin probe setup, where negative surface photovoltage corresponds to negative charge, and vice versa.[47,48] Surface photovoltage data for all films studied here are shown in Figure 3b.

For all temperatures, both $Al_2O_3$ and $HfO_2$ had negative surface photovoltage, while $SiO_2$ had a positive surface photovoltage after annealing ≥450 °C. The magnitude of positive charge in $SiO_2$ is known to increase with thermal annealing,[12] so this observation is in keeping with results from the literature for ultra-thin films. Although the negative charge of $Al_2O_3$ and positive fixed charge of $SiO_2$ are well-reported,[26] the polarity of the fixed charge within $HfO_2$ is less clear. Several studies into ALD growth of $HfO_2$ report the presence of fixed positive charge,[13,31–33] while others disagree.[14,19] Differing charge polarities may be a consequence of the deposition conditions. Many reports on ALD-grown $HfO_2$ involve thermal ALD, with positive fixed charges being observed using tetrakis(methylethylamide) hafnium and trimethylhafnium precursors,[13,31,33] and negative charges being reported with tetrakis(dimethylamido)hafnium,[14] trimethylhafnium,[19] and hafnium tetrachloride[34] precursors. $HfO_2$ deposited under our conditions has the same charge polarity as $Al_2O_3$, that is negatively charged. This agrees well with findings of Aubreit et al.[34]

The magnitude of the surface photovoltage can be indicative of the quantity of charge present but results can be highly variable and dependent on both material properties and surface defects.[34,49] Thus, we applied positive corona charging to characterize the negative fixed charge present in $Al_2O_3$ and $HfO_2$ more reliably. Applying extrinsic positive charge ($Q_{corona}$) via corona charging counteracts the built-in negative charges, thereby neutralizing the contribution of field effects,


© 2022 The Authors. Advanced Materials Interfaces published by Wiley-VCH GmbH

21967350, 2022, 28, Downloaded from https://onlinelibrary.wiley.com/doi/10.1002/admi.202201339 by Oxford University, Wiley Online Library on [21/09/2023]. See the Terms and Conditions (https://onlinelibrary.wiley.com/terms-and-conditions) on Wiley Online Library for rules of use; OA articles are governed by the applicable Creative Commons License

21967350, 2022, 28, Downloaded from https://onlinelibrary.wiley.com/doi/10.1002/admi.202201339 by Oxford University, Wiley Online Library on [21/09/2023]. See the Terms and Conditions (https://onlinelibrary.wiley.com/terms-and-conditions) on Wiley Online Library for rules of use; OA articles are governed by the applicable Creative Commons License

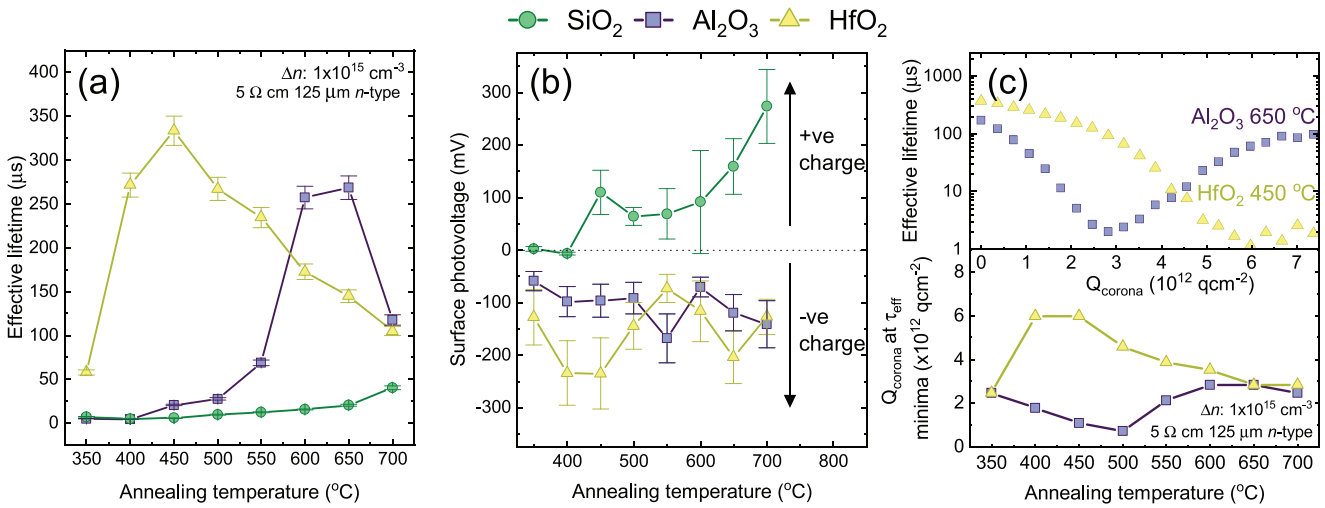


**Figure 3.** a) Effective lifetimes $\tau_{eff}$ at an excess carrier density of $1 \times 10^{15}$ cm$^{-3}$. Effective lifetime values are the average of five measurements, and are assumed to be accurate to ±8%.[44]; b) surface photovoltage. Kelvin probe data are presented as the mean ± one standard deviation. For each sample, at least two locations are measured, and the reported SPV for each point determined is the mean SPV calculated for each darkness-illumination measurement cycle. The error bars are the mean standard deviation of these measurements. c) Corona charging ≈125 µm thick 5 Ω cm *n*-type silicon wafers passivated with 2.2 nm $SiO_2$ (green circles), 0.7 nm $Al_2O_3$ (purple squares), and 0.9 nm $HfO_2$ (yellow triangles). c) Top: Effective lifetime as a function of $Q_{corona}$ for $HfO_2$ and $Al_2O_3$ annealed at the best performing temperatures (450 and 650 °C, respectively). Bottom: $Q_{corona}$ at which $\tau_{eff}$ minima are reached for $Al_2O_3$ (purple squares) and $HfO_2$ (yellow triangles) as a function of annealing temperature.

reducing overall passivation quality, and decreasing effective lifetimes.[50,51] When the field-effect contribution is counterbalanced, only chemical passivation remains. Further charge deposition then gives rise to new field-effect passivation and hence a minimum lifetime value is indicative of the built-in charge. The remaining $\tau_{eff}$ at the minimum is directly related to the level of chemical passivation.[52] A summary of $Q_{corona}$ required to reach this lifetime minimum is demonstrated in Figure 3c, alongside results for two samples showing the impact of successive corona charging on $\tau_{eff}$. In both cases, successive corona treatment reduced the measured effective lifetime to near zero, suggesting very low levels of chemical passivation are present for samples prepared under these conditions.[52] Effective lifetime data as a function of corona charging $Al_2O_3$ and $HfO_2$ at all annealing temperatures considered here can be found in Figure S4, Supporting Information. For the majority of films, once successive corona treatment reduced the measured effective lifetime to near zero, further corona charging resulted in new field effect passivation and hence increased $\tau_{eff}$. However, for $Al_2O_3$ and $HfO_2$ annealed below ≈450–500 °C, it was not possible to increase $\tau_{eff}$ with further corona charging once this minimum was reached, suggesting significant charge leakage. This is unlikely to be due to any crystallization which occurs for $HfO_2$ at these temperatures,[13,14,31] as leakage is also observed for $Al_2O_3$, which does not crystallize at these temperatures. Due to this charge leakage, there is uncertainty in the absolute values of $Q_{corona}$ required to reach a lifetime minimum, particularly at low annealing temperatures. Consequently, in this study, trends in $Q_{corona}$ as a function of annealing temperature will be considered, rather than absolute values.

The level of corona charging required to neutralize each $HfO_2$ film followed a similar trend to the effective lifetime data shown in Figure 3a. This suggests the observed variation in passivation quality with annealing temperature is linked to differing levels of field-effect passivation. Annealing at 400–450 °C gave rise to the highest measured lifetimes (indicating quality of passivation), and also required the greatest extent of corona charge ($6.0 \times 10^{12}$ q cm$^{-2}$) of all $HfO_2$ samples before a $\tau_{eff}$ minimum was reached. This implies a negative fixed charge $Q_{fixed}$ within the dielectric of a similar magnitude, in keeping with previous studies, which report $Q_{fixed}$ values on the order of $10^{11}$–$10^{12}$ cm$^{-2}$.[14,19,34]

Compared to $HfO_2$, there is less agreement between effective lifetime and $Q_{corona}$ trends with temperature for thin $Al_2O_3$ films, except for $Al_2O_3$ annealed at 650 °C, which corresponds to a maximum of both effective lifetime and $Q_{corona}$. $Q_{corona}$ required to neutralize each $Al_2O_3$ sample range from $7.2 \times 10^{11}$–$2.5 \times 10^{12}$ q cm$^{-2}$ and are generally lower than values for equivalent $HfO_2$ samples. For thick dielectrics, $Al_2O_3$ is reported to have higher $Q_{fixed}$ levels than $HfO_2$ ($10^{12}$–$10^{13}$ versus $10^{11}$–$10^{12}$),[14,17–19,34,53] but Figure 2d,e demonstrates that thin and thick $Al_2O_3$ films behave quite differently.

Based on both passivation quality and a reasonable level of fixed negative charge, $HfO_2$ appears extremely promising for hole-selective passivating contacts. In Figure 2, the passivation quality of ultra-thin and ≈20 nm films were compared, and the passivation quality found to be similar. This contrasts with the previous work of Cui et al. and Gope et al., who report an increase in SRV with films greater than ≈15 nm.[13,32] However, as we have so far only considered two extremes of thickness, it may be the case that different behavior is observed at intermediate thicknesses. In order to study the thickness dependence of $HfO_2$ passivation, $HfO_2$ was deposited on both the front and rear of silicon wafers at regular intervals of ALD cycles between 10 (corresponding to 0.9 nm) and 170 (corresponding to ≈20 nm). All samples for this thickness variation study were annealed at 450 °C, the optimum annealing temperature for 0.9 nm films (Figure 3). Post-anneal, effective lifetimes were recorded, as shown in **Figure 4**a.


© 2022 The Authors. Advanced Materials Interfaces published by Wiley-VCH GmbH

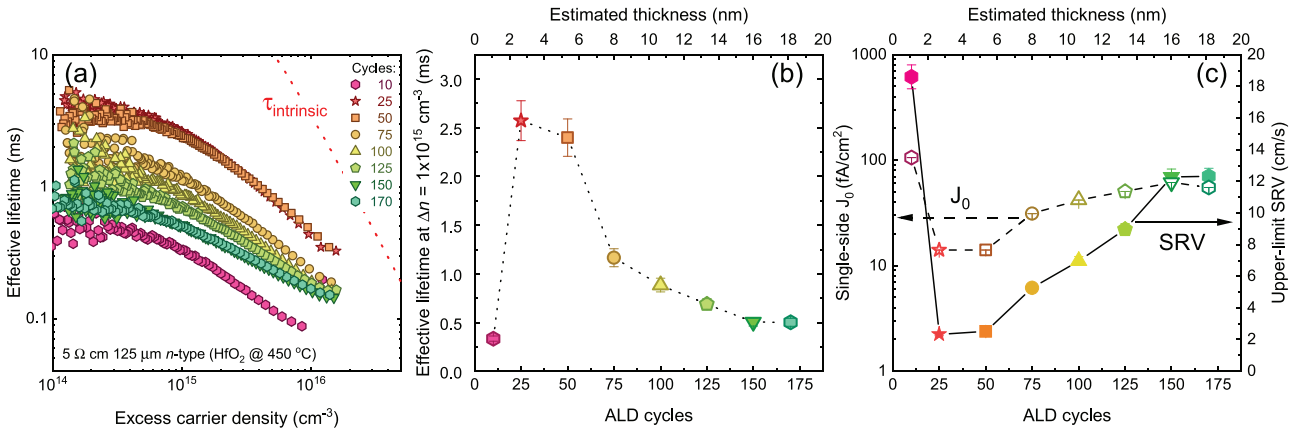


**Figure 4.** Data for $HfO_2$ film growth with different numbers of ALD cycles on both sides of ≈125 µm thick 5 Ω cm n-type silicon wafer samples annealed at 450 °C. a) Effective lifetime versus excess carrier density, with the intrinsic lifetime limit[46] also shown. Effective lifetime curves are the average of five measurements. b) Effective lifetimes extracted at an excess carrier density of $1 \times 10^{15}$ $cm^{-3}$. Effective lifetime values are the average of five measurements, and are assumed to be accurate to ±8%.[44] c) Calculated single-side $J_0$ and upper-limit SRVs. The relative uncertainty of $J_0$ is taken as 10%, based on the work of Kane and Swanson.[54] SRV error bars are based on relative uncertainties of lifetime measurements and wafer thickness.[44]

Although 10 cycles of $HfO_2$ gave the most promising results in Figure 3, further improvements in surface passivation can be made by increasing the number of cycles to 25 or 50. XPS analysis determined that 25 and 50 cycles correspond to a film thickness of 2.2 and 3.3 nm respectively.[37] Parameters used in this calculation can be found in Table S3, Supporting Information. The calculated thickness for 50 cycles of $HfO_2$ (3.3 nm) is lower than would be expected based on the growth rate of $HfO_2$ via ALD under the conditions used in this work (≈1 Å per cycle). Based on the deposition rate of $HfO_2$, the expected thickness of 50 cycles of $HfO_2$ (≈5.0 nm) exceeds the attenuation length of photoelectrons in $HfO_2$ (2.17 nm). Hence, the thickogram method may not be appropriate for layers of this thickness.

The comparatively higher lifetimes recorded for silicon coated with 25 cycles of $HfO_2$ relative to the 10 cycles of $HfO_2$ could be attributed to initial inhomogeneity in $HfO_2$ growth. ALD of $HfO_2$ is known to involve island-like growth at initial stages, although with increasing cycles this inhomogeneity is mitigated.[55] This could potentially explain the improved passivation observed for silicon coated with 25 cycles of $HfO_2$ relative to 10 cycles. Although island growth is (generally) problematic for passivation, for passivating contacts this is less of an issue, as island growth/pinholes can facilitate charge transport.[56]

Passivation quality can be quantified in terms of surface recombination velocity, SRV, defined according to:

$$\mathrm{SRV} = \frac{W}{2}\left(\frac{1}{\tau_{\mathrm{eff}}} - \frac{1}{\tau_{\mathrm{bulk}}}\right) \quad (1)$$

where $W$ is the sample thickness, and $\tau_{\mathrm{eff}}$ and $\tau_{\mathrm{bulk}}$ are the effective and bulk carrier lifetimes, respectively. Alternatively, passivation quality can be described using the recombination current density, $J_0$, which is related to SRV by:[57]

$$\mathrm{SRV} = J_0\left(\frac{N_b + \Delta n}{q n_i^2}\right) \quad (2)$$

where $N_b$ is the bulk dopant concentration, $\Delta n$ is the excess carrier concentration, $q$ is the elementary charge, and $n_i$ is the intrinsic carrier density of Si.

Effective lifetime data extracted at an excess carrier density of $1 \times 10^{15}$ $cm^{-3}$ were used to calculate upper-limit SRVs using Equation (1), while $J_0$ values were determined from the injection-dependent lifetime curves by the Sinton software around the same carrier density, using the Niewelt model.[46,54] The SRVs determined here for 25 and 50 cycles of $HfO_2$ are similar to the best reported SRVs for passivation with thicker $HfO_2$ films,[13,33] especially considering the impact of applying the newest model for intrinsic recombination.[46] $Al_2O_3$ passivation regularly achieves SRVs <1 cm $s^{-1}$,[15] yet for thin films, $HfO_2$ outperforms $Al_2O_3$, as shown in Table S2, Supporting Information. To maximize c-Si solar cell efficiency, $J_0$ needs to be minimized,[4] with good passivating contacts generally having $J_0$ values of ≪10 fA $cm^{-2}$.[4,20] Although the optimum $J_0$ values calculated here based on the Niewelt model are marginally greater than 10 fA $cm^{-2}$, these results were obtained without any post-deposition hydrogenation, common for passivating contacts.[3,9,12] Hence the determined $J_0$ values suggest $HfO_2$ has potential as a material for passivating contacts, and this is a topic of ongoing research.

The decrease in passivation quality above a certain thickness (here 50 cycles, corresponding to 3.3 nm) agrees with the previous work of Cui et al. and Gope et al.[13,32] Gope et al. observe that decreasing passivation quality with increasing film thickness coincides with an increase in interface trap density ($D_{it}$).[32] In our work, the lifetime curves in each case have a similar shape, suggesting there is no significant change in the type of passivation (i.e., chemical or field effects) at play. The variation in effective lifetime with annealing must then be due to differing levels of each component.

This is further demonstrated through corona charging, the results of which are summarized in **Figure 5**. The $Q_{\mathrm{corona}}$ required to reach an effective lifetime minimum indicates the level of field-effect passivation present, where the value of said minima indicates the extent of chemical passivation


© 2022 The Authors. Advanced Materials Interfaces published by Wiley-VCH GmbH

21967350, 2022, 28, Downloaded from https://onlinelibrary.wiley.com/doi/10.1002/admi.202201339 by Oxford University, Wiley Online Library on [21/09/2023]. See the Terms and Conditions (https://onlinelibrary.wiley.com/terms-and-conditions) on Wiley Online Library for rules of use; OA articles are governed by the applicable Creative Commons License

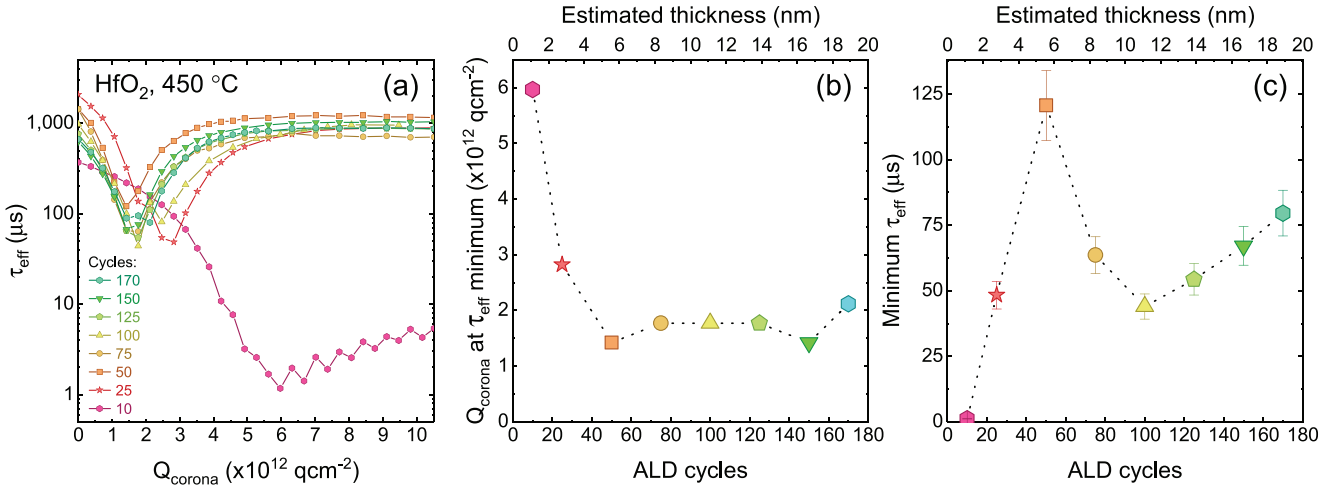


**Figure 5.** a) Corona charging as a function of film thickness (ALD cycles). Effective lifetime values are the average of five measurements. b) $Q_{corona}$ at $\tau_{eff}$ minimum as a function of film thickness. c) Minimum $\tau_{eff}$ following corona charging. Minimum $\tau_{eff}$ values are the average of five measurements and are assumed to be accurate to ±11%.[44] Estimated thicknesses determined by extrapolating from calculated thicknesses of 10/25/50 cycles of $HfO_2$.

present.[51,52] Successive corona charging of each sample was conducted, with the $Q_{corona}$ required and $\tau_{eff}$ at the point where the intrinsic charge is counterbalanced shown in Figure 5b,c, respectively. For the majority of films, once this minimum was reached, further corona charging resulted in new field effect and hence increased $\tau_{eff}$. Only the thinnest film (10 cycles/0.9 nm) suffered from substantial charge leakage, and it was not possible to increase $\tau_{eff}$ with further corona charging once this minimum was reached.

The greatest extent of negative charge was present for the thinnest (0.9 and 2.2 nm) $HfO_2$ samples, whereas for thicker samples the level of built-in negative charge was similar. For these samples, $Q_{corona}$ required was $\approx 1.4 \times 10^{12}$ q cm$^{-2}$, agreeing with the work of Gougam et al. who report similar values for films of equivalent thickness.[33] With increasing film thickness, there was an initial increase in chemical passivation, peaking at 50 cycles (3.3 nm). Beyond this point, chemical passivation initially decreased, followed by a second gradual increase. This gradual increase in chemical passivation at thicknesses above 5 nm contrasts with the work of Gope et al., who observe decreasing chemical passivation when film thickness increases beyond 8 nm.[32]

## 3. Conclusions

This study determined the passivating qualities of ultra-thin layers of ALD-grown $SiO_2$, $Al_2O_3$, and $HfO_2$. $HfO_2$ was found to offer very good levels of passivation despite nanometer level thicknesses, with an SRV of 18.6 cm s$^{-1}$ achieved for films 0.9 nm thick. Passivation can be improved by increasing film thickness to 2.2 nm, resulting in SRVs <2.5 cm s$^{-1}$, among the best reported for $HfO_2$ films. The passivation quality of $HfO_2$ is strongly dependent on post-deposition activation temperature, with the best performance arising from annealing in air at 450 °C. The high-quality passivation achievable translates to low single-sided $J_0$ values (14 fA cm$^{-2}$), suggesting $HfO_2$ has potential as a material for passivating contacts. As the passivation is achieved at temperatures <500 °C, this provides a potential route to reduce the thermal budget required for passivating contacts, by utilizing dielectrics grown by ALD. The $HfO_2$ films grown in this work have been demonstrated, through surface photovoltage measurements and corona charging, to possess negative fixed charges on the order of $10^{12}$ q cm$^{-2}$. Consequently, the $HfO_2$ nanolayers reported here show great promise for hole-selective contact implementations.

## 4. Experimental Section

*Materials*: Substrates for lifetime and Kelvin probe measurements were high quality, ≈125 µm thick, (100) orientation, 5 Ω cm, chemically etched *n*-type Czochralski silicon wafers. The ALD precursors used to deposit $SiO_2$, $Al_2O_3$ and $HfO_2$ were bis(diethylamido) silane, trimethylaluminum, and tetrakis(dimethylamido)hafnium, respectively.

*Sample Preparation*: Silicon substrates were prepared following a previously reported chemical cleaning and etching procedure.[58] The final step in the cleaning process (immersion in 2% HF for 60 s) was modified to immersion in 1% HF/1% HCl for 5 min, as this has been found to improve passivation quality.[15] Coatings were grown via plasma-enhanced ALD using a Veeco Fiji G2 system with an external load lock. Films were deposited at 200 °C using $O_2$ plasma. Growth rates per cycle were reported to be ≈0.6 Å ($SiO_2$), ≈1.3 Å ($Al_2O_3$), and ≈1 Å ($HfO_2$).[35] Films were deposited on both sides of each wafer. A post-deposition anneal in air was performed for 30 min in a quartz tube furnace.

*Characterization*: XPS data were collected at the Photoemission Research Technology Platform, University of Warwick, using a Kratos Axis Ultra DLD spectrometer. Samples were mounted on a non-magnetic, stainless steel bar using electrically conductive carbon tape. The base pressure of the XPS spectrometer was ≈$1 \times 10^{-10}$ mbar, and samples were pumped to below $1 \times 10^{-6}$ mbar in the load lock before transfer. XPS measurements were performed using a monochromated Al K$\alpha$ X-ray (1.487 keV) source. Measurements were conducted at room temperature and at a take-off angle of 90° with respect to the sample surface. The core level spectra were recorded by using a pass energy of 40 eV from an analysis area of 300 µm × 700 µm. Fitting procedures to extract peak positions and relative stoichiometries were performed using the Casa XPS software suite, linear backgrounds, and mixed Gaussian–Lorentzian (Voigt) line shapes. These were fitted and corrected using their corresponding sensitivity factors, taking the mean free path of the


© 2022 The Authors. Advanced Materials Interfaces published by Wiley-VCH GmbH

21967350, 2022, 28, Downloaded from https://onlinelibrary.wiley.com/doi/10.1002/admi.202201339 by Oxford University, Wiley Online Library on [21/09/2023]. See the Terms and Conditions (https://onlinelibrary.wiley.com/terms-and-conditions) on Wiley Online Library for rules of use; OA articles are governed by the applicable Creative Commons License

21967350, 2022, 28, Downloaded from https://onlinelibrary.wiley.com/doi/10.1002/admi.202201339 by Oxford University, Wiley Online Library on [21/09/2023]. See the Terms and Conditions (https://onlinelibrary.wiley.com/terms-and-conditions) on Wiley Online Library for rules of use; OA articles are governed by the applicable Creative Commons License

photoelectrons and photoionization cross sections of these core levels into account.

Film thicknesses were determined via the thickogram method.[37] Thickness determination was generally conducted on XPS spectra of annealed samples, except in the case of $HfO_2$. $HfO_2$ thicknesses were determined from XPS spectra of as-deposited samples, due to the attenuation lengths needed to calculate thickness corresponding to as-deposited $HfO_2$.[41] The impact of annealing $HfO_2$ on recorded XPS spectra is also discussed in Section S1, Supporting Information.

Photoconductance decay lifetime measurements were performed at room temperature using a Sinton WCT-120 lifetime tester with a 2 cm diameter coil. Measurements were performed using the quick decaying flash mode, except for low effective lifetime samples, which were measured using the slow-decaying flash. Results were averaged over five measurements. Lifetime measurements were made on $5 \times 5$ cm samples, which were sufficiently large to avoid strong edge recombination effects.[59] Effective lifetime measurements were assumed to be accurate to ±8%.[44]

Passivation level can additionally be quantified in terms of a surface recombination velocity, SRV, defined according to Equation (1). The bulk lifetime was determined by intrinsic (i.e., radiative and Auger) and extrinsic recombination. Intrinsic recombination was quantified using the parametrization of Niewelt et al.,[46] taking photon recycling into account by assuming planar sample surfaces. Values of SRV reported here were upper limits as it was assumed for the evaluation that there were no sources of extrinsic recombination other than the surface. Values for the recombination current density ($J_0$) were determined by the Sinton WCT-120 software (version 5.74) which uses an approach similar to that of Kane and Swanson, and has an uncertainty of less than 10%.[54] The samples were assumed to have identical films on both the front and the rear side. Hence single-side $J_0$ values were obtained by dividing extracted $J_0$ by 2.[9]

Contact potential difference (CPD) measurements were made with a KP Technologies SKP5050 Kelvin Probe with a 2 mm gold-plated tip, based on the method of Baikie et al.[60] A Fiber-Lite DC-950 Quartz Tungsten Halide lamp was used for surface photovoltage measurements. The light intensity measured at the sample location with a Thorlabs PM16-130 power meter was 12.22 W $cm^{-2}$ at 635 nm. Surface photovoltage is defined as $CPD_{illumination} - CPD_{dark}$.

Corona charging was used to characterize the level of negative fixed charge in the dielectric films. A custom-built corona charge apparatus, similar to that described by Bonilla et al.[61] was used to deposit charge on the oxide thin films. The corona charge apparatus consisted of a sharp needle held at ≈7 kV and positioned 7 cm from the sample. Samples were subjected to 3.5 V for 5 seconds on either side. The charge deposition rate was determined according to the Kelvin Probe method of Bonilla et al.,[62] which demonstrated 5 s of corona charging corresponded to deposited charge $Q_{corona}$ of $\approx 3.7 \times 10^{11}$ q $cm^{-2}$. Following each corona charge, effective lifetime was measured in generalized mode, and results averaged over five measurements. Effective lifetime measurements made under these conditions were assumed to be accurate to ±11%.[44]

*Statistical Analysis*: The results discussed in this paper were based on a total sample size of $n = 48$. (Thin = $8 \times SiO_2$ samples, $8 \times Al_2O_3$ samples, $8 \times HfO_2$ samples. Thick = $6 \times SiO_2$ samples, $6 \times Al_2O_3$ samples, $6 \times HfO_2$ samples. $HfO_2$ thickness variation = $6 \times$ additional samples.) Thicknesses determined from XPS data were assumed to be accurate to ±10%, based on the uncertainty in reported values of attenuation length.[37] All effective lifetime data presented were the average of five measurements. Effective lifetime measurements made under transient conditions were assumed to have an error bar of ±8%,[44] whilst those made under generalized conditions have an uncertainty of ±11%.[44] The relative uncertainty of surface recombination velocity was based on error propagation of relative uncertainty of lifetime measurements and wafer thickness (uncertainty = 1 standard deviation of measured thicknesses). $J_0$ values were assumed to have an error of less than 10%.[54] Kelvin probe data were presented as the mean ± one standard deviation. For each sample, at least two locations were measured, and the reported SPV for each point determined was the mean SPV calculated for each darkness-illumination measurement cycle.

## Supporting Information

Supporting Information is available from the Wiley Online Library or from the author.

## Acknowledgements

S.L.P. and A.W. acknowledge funding from the Engineering and Physical Sciences Research Council (EPSRC) Doctoral Training Partnership (EP/R513374/1). Work was supported by the EPSRC Charged Oxide Inversion Layer (COIL) solar cells project (EP/V037749/1 and EP/V038605/1), the Leverhulme Trust (RPG-2020-377), and the Royal Society (RGS\R2\212150). R.S.B. was supported by the Royal Academy of Engineering under the Research Fellowship scheme. For the purpose of open access, the authors have applied a Creative Commons Attribution (CC BY) license to any Author Accepted Manuscript version arising from this submission.

## Conflict of Interest

The authors declare no conflict of interest.

## Author Contributions

The project concept was devised by S.L.P., N.E.G., and J.D.M. Experimental work, sample processing, characterization, and data analysis were largely conducted by S.L.P. The XPS data used in this study were collected and analyzed by E.K. G.J.P.F., M.W., and L.F.J.P. assisted with XPS measurements and access. The corona charging apparatus used in this work was designed and fabricated by B.W. and N.E.G., with technical guidance from R.S.B. A.W. assisted with development of $HfO_2$ passivation. E.K., T.N., N.E.G., and J.D.M. contributed to discussions and data analysis. The manuscript was written by S.L.P., with input from J.D.M., N.E.G., T.N., E.K., and R.S.B.

## Data Availability Statement

Data underpinning figures in this paper can be freely downloaded from http://wrap.warwick.ac.uk/167970/. Requests for additional data should be made directly to the corresponding authors.

## Keywords

Atomic layer deposition, dielectrics, hafnium oxide, passivation, silicon

Received: June 15, 2022
Revised: July 13, 2022
Published online: September 4, 2022

[1] M. Fischer, M. Woodhouse, S. Herritsch, J. Trube, *International Technology Roadmap for Photovoltaic (ITRPV)*, VDMA, Frankfurt, Germany **2022**.

[2] J. Benick, B. Hoex, M. C. M. van de Sanden, W. M. M. Kessels, O. Schultz, S. W. Glunz, *Appl. Phys. Lett.* **2008**, *92*, 253504.


© 2022 The Authors. Advanced Materials Interfaces published by Wiley-VCH GmbH

[3] T. G. Allen, J. Bullock, X. Yang, A. Javey, S. De Wolf, *Nat. Energy* **2019**, *4*, 914.
[4] J. Melskens, B. W. H. van de Loo, B. Macco, L. E. Black, S. Smit, W. M. M. Kessels, *IEEE J. Photovolt.* **2018**, *8*, 373.
[5] E. Khorani, S. McNab, T. E. Scheul, T. Rahman, R. S. Bonilla, S. A. Boden, P. R. Wilshaw, *APL Mater.* **2020**, *8*, 111106.
[6] P. Stradins, S. Essig, W. Nemeth, B. G. Lee, D. Young, A. Norman, Y. Liu, J. W. Luo, E. Warren, A. Dameron, V. LaSalvia, M. Page, A. Rohatgi, A. Upadhyaya, B. Rounsaville, Y. W. Ok, S. Glunz, J. Benick, F. Feldmann, M. Hermle, presented at *The WCPEC-6: 6th World Conference on Photovoltaic Energy Conversion*, Kyoto, Japan, November **2014**.
[7] F. Feldmann, M. Bivour, C. Reichel, M. Hermle, S. W. Glunz, *Sol. Energy Mater. Sol. Cells* **2014**, *120*, 270.
[8] F. Haase, C. Hollemann, S. Schäfer, A. Merkle, M. Rienäcker, J. Krügener, R. Brendel, R. Peibst, *Sol. Energy Mater. Sol. Cells* **2018**, *186*, 184.
[9] D. Kang, H. C. Sio, J. Stuckelberger, D. Yan, S. P. Phang, R. Liu, T. N. Truong, T. Le, H. T. Nguyen, X. Zhang, D. Macdonald, *Prog. Photovolt.: Res. Appl.* **2022**, *30*, 970.
[10] A. Ingenito, G. Nogay, Q. Jeangros, E. Rucavado, C. Allebé, S. Eswara, N. Valle, T. Wirtz, J. Horzel, T. Koida, M. Morales-Masis, M. Despeisse, F.-J. Haug, P. Löper, C. Ballif, *Nat. Energy* **2018**, *3*, 800.
[11] F. Feldmann, M. Simon, M. Bivour, C. Reichel, M. Hermle, S. W. Glunz, *Appl. Phys. Lett.* **2014**, *104*, 181105.
[12] C. Reichel, F. Feldmann, A. Richter, J. Benick, M. Hermle, S. W. Glunz, *Prog. Photovolt.: Res. Appl.* **2022**, *30*, 288.
[13] J. Cui, Y. Wan, Y. Cui, Y. Chen, P. Verlinden, A. Cuevas, *Appl. Phys. Lett.* **2017**, *110*, 021602.
[14] X. Cheng, P. Repo, H. Halvard, A. P. Perros, E. S. Marstein, M. Di Sabatino, H. Savin, *IEEE J. Photovolt* **2017**, *7*, 479.
[15] N. E. Grant, A. I. Pointon, R. Jefferies, D. Hiller, Y. Han, R. Beanland, M. Walker, J. D. Murphy, *Nanoscale* **2020**, *12*, 17332.
[16] A. Richter, S. W. Glunz, F. Werner, J. Schmidt, A. Cuevas, *Phys. Rev. B* **2012**, *86*, 165202.
[17] B. Hoex, J. Schmidt, P. Pohl, M. C. M. van de Sanden, W. M. M. Kessels, *J. Appl. Phys.* **2008**, *104*, 044903.
[18] B. Hoex, S. B. B. Heil, E. Langereis, M. C. M. van de Sanden, W. M. M. Kessels, *Appl. Phys. Lett.* **2006**, *89*, 042112.
[19] F. Lin, B. Hoex, Y. H. Koh, J. Lin, A. G. Aberle, *ECS J. Solid State Sci. Technol.* **2013**, *2*, N11.
[20] F. Feldmann, G. Nogay, J.-I. Polzin, B. Steinhauser, A. Richter, A. Fell, C. Schmiga, M. Hermle, S. W. Glunz, *IEEE J. Photovolt.* **2018**, *8*, 1503.
[21] R. Peibst, U. Römer, Y. Larionova, M. Rienäcker, A. Merkle, N. Folchert, S. Reiter, M. Turcu, B. Min, J. Krügener, D. Tetzlaff, E. Bugiel, T. Wietler, R. Brendel, *Sol. Energy Mater. Sol. Cells* **2016**, *158*, 60.
[22] U. Würfel, A. Cuevas, P. Würfel, *IEEE J. Photovolt* **2015**, *5*, 461.
[23] R. Brendel, R. Peibst, *IEEE J. Photovolt* **2016**, *6*, 1413.
[24] M. Köhler, M. Pomaska, P. Procel, R. Santbergen, A. Zamchiy, B. Macco, A. Lambertz, W. Duan, P. Cao, B. Klingebiel, S. Li, A. Eberst, M. Luysberg, K. Qiu, O. Isabella, F. Finger, T. Kirchartz, U. Rau, K. Ding, *Nat. Energy* **2021**, *6*, 529.
[25] B. W. H. van de Loo, B. Macco, J. Melskens, M. A. Verheijen, W. M. M. Kessels, in *IEEE 43rd Photovoltaics Specialists Conference (PVSC)*, IEEE, Piscataway, NJ **2016**, pp. 3655–3660.
[26] R. S. Bonilla, B. Hoex, P. Hamer, P. R. Wilshaw, *Phys. Status Solidi A* **2017**, *214*, 1700293.
[27] S. W. Glunz, D. Biro, S. Rein, W. Warta, *J. Appl. Phys.* **1999**, *86*, 683.
[28] G. Dingemans, W. M. M. Kessels, *J. Vac. Sci. Technol., A* **2012**, *30*, 040802.
[29] S. W. Glunz, F. Feldmann, *Sol. Energy Mater. Sol. Cells* **2018**, *185*, 260.
[30] J. Schmidt, F. Werner, B. Veith, D. Zielke, S. Steingrube, P. P. Altermatt, S. Gatz, T. Dullweber, R. Brendel, *Energy Procedia* **2012**, *15*, 30.
[31] F. Lin, B. Hoex, Y. Koh, J. Lin, A. Aberle, *Energy Procedia* **2012**, *15*, 84.
[32] J. Gope, Vandana, N. Batra, J. Panigrahi, R. Singh, K. K. Maurya, R. Srivastava, P. K. Singh, *Appl. Surf. Sci.* **2015**, *357*, 635.
[33] A. B. Gougam, B. Rajab, A. B. Afif, *Mater. Sci. Semicond. Process.* **2019**, *95*, 42.
[34] V. Aubriet, K. Courouble, M. Gros-Jean, Ł. Borowik, *Rev. Sci. Instrum.* **2021**, *92*, 083905.
[35] Veeco Data Sheets, **2015**.
[36] G. He, X. Chen, Z. Sun, *Surf. Sci. Rep.* **2013**, *68*, 68.
[37] P. J. Cumpson, *Surf. Interface Anal.* **2000**, *29*, 403.
[38] Z. Yang, J. Krugener, F. Feldmann, J.-I. Polzin, B. Steinhauser, T. T. Le, D. Macdonald, A. Liu, *Adv. Energy Mater.* **2022**, *12*, 2103773.
[39] D. Hiller, P. Hönicke, D. König, *Sol. Energy Mater. Sol. Cells* **2020**, *215*, 110654.
[40] A. Liu, Z. Yang, F. Feldmann, J.-I. Polzin, B. Steinhauser, S. P. Phang, D. Macdonald, *Sol. Energy Mater. Sol. Cells* **2021**, *230*, 111254.
[41] S. Tougaard, QUASES-IMFP-TPP2MM, **2016**. [Online]. Available: http://www.quases.com/products/quases-imfp-tpp2m/.
[42] S. Tanuma, C. J. Powell, D. R. Penn, *Surf. Interface Anal.* **1994**, *21*, 165.
[43] G. Dingemans, C. Van Helvoirt, M. C. M. van de Sanden, W. M. Kessels, *ECS Trans.* **2011**, *35*, 191.
[44] A. L. Blum, J. S. Swirhun, R. A. Sinton, F. Yan, S. Herasimenka, T. Roth, K. Lauer, J. Haunschild, B. Lim, K. Bothe, Z. Hameiri, B. Seipel, R. Xiong, M. Dhamrin, J. D. Murphy, *IEEE J. Photovolt.* **2014**, *4*, 525.
[45] M. Pawlik, J. P. Vilcot, M. Halbwax, D. Aureau, A. Etcheberry, A. Slaoui, T. Schutz-Kuchly, R. Cabal, *Energy Procedia* **2014**, *60*, 85.
[46] T. Niewelt, B. Steinhauser, A. Richter, B. Veith-Wolf, A. Fell, B. Hammann, N. E. Grant, L. Black, J. Tan, A. Youssef, J. D. Murphy, J. Schmidt, M. C. Schubert, S. W. Glunz, *Sol. Energy Mater. Sol. Cells* **2022**, *235*, 111467.
[47] L. Kronik, Y. Shapira, *Surf. Sci. Rep.* **1999**, *37*, 1.
[48] R. S. Bonilla, *Mater. Res. Exp.* **2022**, *9*, 085901.
[49] R. J. Hamers, K. Markert, *Phys. Rev. Lett.* **1990**, *64*, 1051.
[50] B. Hoex, J. Schmidt, M. C. M. van de Sanden, W. M. M. Kessels, presented at the *33rd IEEE Photovoltaic Specialist Conference (PVSEC 2008)*, California, USA May **2008**.
[51] F. Ji, C. Zhou, X. Jia, L. Gong, J. Zhu, W. Wang, *Chem. Phys. Lett.* **2019**, *730*, 60.
[52] Y. Zhao, C. Zhou, X. Zhang, P. Zhang, Y. Dou, W. Wang, X. Cao, B. Wang, Y. Tang, S. Zhou, *Nanoscale Res. Lett.* **2013**, *8*, 114.
[53] J. Gao, G. He, D. Xiao, P. Jin, S. Jiang, W. Li, S. Liang, L. Zhu, *J. Mater. Res. Technol.* **2017**, *33*, 901.
[54] D. E. Kane, R. M. Swanson, presented at the *18th IEEE Photovoltaic Specialists Conference*, Las Vegas, NV, October **1985**.
[55] H. S. Chang, H. Hwang, *Appl. Phys. Lett.* **2005**, *86*, 031906.
[56] H. Guthrey, C. Lima Salles, A. S. Kale, W. Nemeth, M. Page, S. Agarwal, D. L. Young, M. Al-Jassim, P. Stradins, *ACS Appl. Mater. Interfaces* **2020**, *12*, 55737.
[57] L. E. Black, in *New Perspectives on Surface Passivation: Understanding the Si-$Al_2O_3$ Interface*, Springer, New York **2016**, p. 27.
[58] N. E. Grant, P. P. Altermatt, T. Niewelt, R. Post, W. Kwapil, M. C. Schubert, J. D. Murphy, *Sol. RRL* **2021**, *5*, 2000754.
[59] M. Kessler, T. Ohrdes, P. P. Altermatt, R. Brendel, *J. Appl. Phys.* **2012**, *111*, 054508.
[60] I. D. Baikie, S. Mackenzie, P. J. Z. Estrup, J. A. Meyer, *Rev. Sci. Instrum.* **1991**, *62*, 1326.
[61] R. S. Bonilla, C. Reichel, M. Hermle, P. Hamer, P. R. Wilshaw, *Appl. Surf. Sci.* **2017**, *412*, 657.
[62] R. S. Bonilla, N. Jennison, D. Clayton-Warwick, K. A. Collett, L. Rangs, P. R. Wilshaw, *Energy Procedia* **2016**, *92*, 326.


© 2022 The Authors. Advanced Materials Interfaces published by Wiley-VCH GmbH

21967350, 2022, 28, Downloaded from https://onlinelibrary.wiley.com/doi/10.1002/admi.202201339 by Oxford University, Wiley Online Library on [21/09/2023]. See the Terms and Conditions (https://onlinelibrary.wiley.com/terms-and-conditions) on Wiley Online Library for rules of use; OA articles are governed by the applicable Creative Commons License